

Transient cavities near boundaries. Part 1. Rigid boundary

By J. R. BLAKE, B. B. TAIB† AND G. DOHERTY

Department of Mathematics, The University of Wollongong, Wollongong,
New South Wales, 2500 Australia.

(Received 14 November 1985 and in revised form 17 March 1986)

The growth and collapse of transient vapour cavities near a rigid boundary in the presence of buoyancy forces and an incident stagnation-point flow are modelled via a boundary-integral method. Bubble shapes, particle pathlines and pressure contours are used to illustrate the results of the numerical solutions. Migration of the collapsing bubble, and subsequent jet formation, may be directed either towards or away from the rigid boundary, depending on the relative magnitude of the physical parameters. For appropriate parameter ranges in stagnation-point flow, unusual 'hour-glass' shaped bubbles are formed towards the end of the collapse of the bubble. It is postulated that the final collapsed state of the bubble may be two toroidal bubbles/ring vortices of opposite circulation. For buoyant vapour cavities the Kelvin impulse is used to obtain criteria which determine the direction of migration and subsequent jet formation in the collapsing bubble.

1. Introduction

Cavitation damage is one of the major problems that may occur in hydraulic machinery, requiring the careful design of equipment to avoid its occurrence or at least allow it to exist in a controlled and hydrodynamically efficient form. Excessive cavitation not only leads to structural damage to the equipment and noise but may also lead to a dramatic decline in operating efficiency. Many graphic examples of cavitation damage to ship propellers, turbine blades, spillways and valves abound in the literature (see e.g. Knapp, Daily & Hammitt 1970; Arndt 1981).

Cavitation bubbles may be created and exist in many different physical circumstances such as in a tip vortex (see e.g. Batchelor 1967, figure 6.12.2(a)), transient or travelling bubbles (figure 6.12.1), sheets of bubbles (figure 6.12.2(b)), steady cavities (figure 6.12.5) and in regions of high turbulent intensity. In turbomachinery a common occurrence would be for cavitation inception to occur just downstream from the point of minimum pressure, but prior to the separation point, so that the cavitation bubbles are swept up over the separation 'bubble'. Structural damage is frequently observed to occur near reattachment of the boundary layer.

There have been extensive experimental studies on cavitating fluids from the more practical engineering side (Knapp *et al.* 1970; Arndt 1981) with less experimental work at the fundamental level, although recent developments with high-speed cameras have enabled accurate photographic records of bubble shape to be obtained (Benjamin & Ellis 1966; Gibson 1968; Lauterborn & Bolle 1975; Lauterborn 1982;

† Current address: Mathematics Department, Universiti Pertanian Malaysia, Serdang, Selangor, Malaysia.

Lauterborn & Vogel 1984). On the other hand notable theoretical studies, including numerical solutions, have been less prevalent.

Most theory to date, apart from purely numerical solutions, has been based on the spherically symmetric solution of a collapsing cavitation bubble, first obtained by Rayleigh (1917). Typically, an asymmetry is introduced in the theory, say for example by a rigid boundary or free surface, and a perturbation analysis is often developed in terms of the small parameter ϵ , which is equal to the ratio of the initial (maximum) radius of the spherical bubble to the distance of the centre from the boundary. As the Rayleigh bubble is normally the zeroth-order solution, these studies yield small perturbations from the Rayleigh solution and thus any inferences on what might happen at the physically important values of ϵ near 1 may be potentially misleading. A recent example of this approach may be found in Chahine & Bovis (1983) wherein further references may be found.

Another notable contribution to the theoretical development of the subject was the paper by Benjamin & Ellis (1966) which combined an intuitive theoretical discussion of cavitation damage together with observations of the gross asymmetries (the high-speed jet) that may occur during cavitation-bubble collapse near a rigid boundary. Probably the most important concept that they introduced into the study of cavitation bubble dynamics was the concept of the Kelvin impulse (see also Lamb 1932). The Kelvin impulse may be interpreted as the linear momentum of the 'bubble' and in many ways is akin to the linear momentum of a projectile. The Kelvin impulse, in unsteady fluid mechanics and in the presence of boundaries, is a conceptually difficult quantity to understand (see Lamb 1932; Benjamin & Ellis, 1966; Blake & Cerone 1982; Blake 1983 for further discussion). Analogous studies in the area of aquatic swimming have been developed by Saffman (1967) and Wu (1976) and in the general area of Lagally's Theorem (see Landweber & Miloh 1980 for further references). Later in this paper we exploit the use of the Kelvin impulse to delineate between the relative importance of boundary interaction and buoyancy effects in determining the direction of movement of a cavitation bubble and the consequent direction of the high-speed liquid jet.

Over the last decade numerical solutions have improved our understanding of cavitation bubble dynamics in enabling us to consider realistic examples of bubbles immediately adjacent to the boundary ($\epsilon \approx 1$). Quantities that may be obtained as a result of these numerical computations include bubble shape as a function of time, particle paths, pressure contours, jet speed and instantaneous streamlines. The first fully numerical paper for the complete collapse of a cavitation bubble near a rigid boundary was developed by Plesset & Chapman (1971) and their results have been the basis for comparisons ever since. Lauterborn & Bolle's (1975) experiments showed remarkable agreement between their experimental study and Plesset & Chapman's theory considering the obvious assumptions in the theory and difficulty in producing equivalent experimental conditions. More detailed studies on cavitation bubbles near rigid boundaries have recently been presented by Guerri, Lucca & Prosperetti (1981), Prosperetti (1982), Cerone & Blake (1984), Taib, Doherty & Blake (1984) and Taib (1985). Numerical studies on a cavitation bubble near a free surface have been developed by Lenoir (1976), Blake & Gibson (1981), Taib (1985), and in a paper in preparation by the present authors.

In our study herein we are primarily concerned with the growth and collapse of cavitation bubbles near rigid boundaries. Bearing in mind that the shape of the bubble is specified by

$$\frac{dx}{dt} = u(x, t), \quad x \in S, \quad (1)$$

where \mathbf{x} is a position vector, S the surface of the bubble, \mathbf{u} the velocity vector and t time, and that for an incompressible and inviscid fluid the velocity is related to the pressure gradient (∇p) by

$$\mathbf{u} = \mathbf{u}_0 - \frac{1}{\rho} \int_{x_0}^{\mathbf{x}} \nabla p \, dt, \quad (2)$$

where ρ is the fluid density, it is clear that any realistic theoretical study must include (i) a rigid boundary, (ii) an ambient velocity field and (iii) an ambient pressure field.

During the growth phase cavitation bubbles are, in many circumstances, approximately spherical, appearing to be almost independent of the local velocity and pressure field, which will be fully three-dimensional. However during collapse the irregularities in the velocity and pressure field together with the presence of the boundary and nearby bubbles will be clearly evident in the bubble shape. While the fully three-dimensional study is not entirely beyond theoretical and machine capabilities, it would seem prudent to study a reduced problem whereby we assume axisymmetry in the flow field and bubble shape. In this way we can compare the relative effects of the interaction of a transient bubble with a rigid boundary and an imposed ambient velocity and pressure field.

In this paper we develop a theory to model the growth and collapse of buoyant vapour bubbles near a rigid boundary in the presence of an axisymmetric stagnation-point flow (a pure straining motion, characterized by a rate-of-strain tensor linearly dependent on the strength of the stagnation-point flow). This allows us to analyse, in isolation and together, the three principle kinematic and dynamical features of cavitation outlined above. The importance of each of these effects may be determined by the magnitude of the dimensionless parameters

$$\gamma = \frac{h}{R_m}, \quad \delta = \pm \left(\frac{\rho g R_m}{\Delta p} \right)^{\frac{1}{2}}, \quad \alpha = \pm c_0 R_m \left(\frac{\rho}{\Delta p} \right)^{\frac{1}{2}}, \quad (3)$$

where h is the initial distance of the bubble centroid from the rigid boundary, R_m is the maximum bubble radius (not to be confused with the initially small bubble radius R_0), g gravitational acceleration and $\Delta p = p_a - p_c$, where p_a is the ambient pressure in the fluid at the initial bubble centroid, p_c is the vapour pressure inside the bubble and c_0 is the strength of the stagnation-point flow. Thus γ determines the initial location of the bubble ($= 1/\epsilon$ from earlier discussion), δ the relative importance of buoyancy forces while α is a measure of the incident stagnation-point flow. The signs in front of δ corresponds to the different directions of the gravity vector while the signs for α correspond to the different directions of the stagnation-point flow (i.e. forward or rearward). The configuration considered in this theoretical study is essentially identical with the experimental arrangement described in Gibson (1968), Blake & Gibson (1981) and Gibson & Blake (1982) and thus provides a basis for comparison.

Before proceeding with the theoretical study it is worthwhile considering the competing physical phenomena that are involved in this study. The Bjerknes effect (see Birkhoff & Zarantonello 1957; Batchelor 1967) for a pulsating cavitation bubble near a rigid boundary is directed towards the rigid boundary, thus the bubble migrates towards the boundary with the consequence that the high-speed liquid jet is also directed towards the boundary (see also experimental studies reported in Benjamin & Ellis 1966; Gibson 1968; Lauterborn & Bolle 1975; Lauterborn 1982).

Buoyancy effects act in the opposite direction to the gravity vector because of the lower density of the vapour inside the bubble. The buoyancy force is directly proportional to the volume of the bubble so that initially in the growth phase and

late in the collapse phase, when the bubble volume is small, buoyancy effects will be less important. However, as around 80% of the lifetime of the bubble is spent near maximum bubble size these effects may be important for bubble diameters greater than 1 cm. Depending on the location of the rigid boundary, buoyancy forces may either oppose or support the Bjerknes effect; both cases are considered in later examples. Buoyancy forces are not normally important in practice, although in experiments involving reduced pressures, bubbles may grow to a size sufficient to make buoyancy forces important.

In stagnation-point flow the maximum pressure occurs at the stagnation point, thus leading us to consider two contributions to the dynamics of the bubble's motion; namely the opposing influence of the velocity and pressure fields at a forward stagnation point corresponding to a deceleration of the fluid as it approaches the stagnation point, while at a rear stagnation point they act in the same direction corresponding to an acceleration of the fluid away from the stagnation point. In addition the relative importance of each contribution is dependent on the distance from the boundary.

Thus, by considering the growth and collapse of cavitation bubbles near a rigid boundary in which buoyancy forces may be important and in the presence of an incident stagnation-point flow, we have competing physical phenomena that contribute to the overall response of the cavitation bubble. An understanding of these basic dynamical contributions will be an invaluable contribution to our understanding of cavitation-bubble dynamics.

In the next section we develop the equations required to model a cavitation bubble near a rigid boundary. This is followed by a brief description of the boundary-integral method which is used to obtain pointwise information on the time-dependent bubble shape, particle paths and pressure field surrounding the bubble. Results of these calculations are interpreted and discussed in the following section. In the penultimate section, some of the earlier results are interpreted in terms of the Kelvin impulse. The final section summarizes the main conclusions that may be drawn from the study and identifies areas for future study.

2. Theory

In this section we develop the theory to model the growth and collapse of a vapour bubble that is subject to both buoyancy forces and the velocity and pressure field due to an axisymmetric stagnation-point flow near a rigid boundary. We assume the flow field and the bubble remain axisymmetric, which experimental evidence tends to support. The geometrical description of the problem is illustrated in figure 1.

The fluid dynamics may be modelled by considering the fluid to be incompressible, inviscid and irrotational leading to the velocity being expressed as the gradient of a potential ϕ , i.e.

$$\mathbf{u} = \nabla\phi, \quad \nabla^2\phi = 0. \quad (4)$$

We neglect viscous forces because of the high velocities and consequent high Reynolds number ($R \sim 10^4$) during growth and collapse. In addition the boundary layers are typically very thin around the stress-free bubble surface, so in any event viscous forces are confined to the immediate proximity of the surface of the bubble. Surface-tension forces are also neglected although they may be important during bubble growth just after inception and also at the jet tip in the latter stages of collapse (e.g. in Blake & Gibson's 1981 experiments at reduced pressure

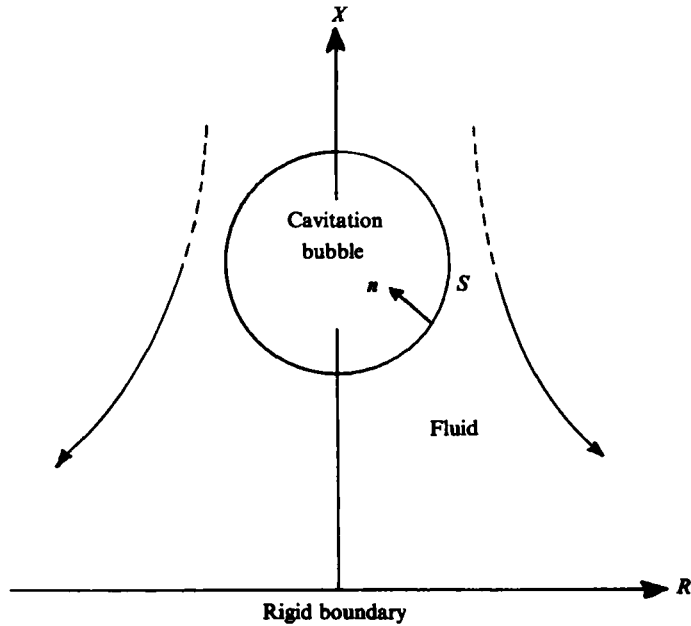


FIGURE 1. Geometry used in the analysis of the growth and collapse of a vapour bubble near a rigid boundary.

$p_0 - p_c = 6-7 \text{ kPa}$, $p_{st} = 1.4 \text{ kPa}$). Compressibility effects are generally unimportant during the first pulsation as velocities are typically significantly less than the speed of sound in either the vapour or the liquid. A more extensive discussion of the above physical factors may be found in Hammitt (1980). Although not normally important in cavitation, buoyancy forces are included to allow us to independently vary the ambient pressure field around the bubble and to monitor its influence on the bubble's growth and collapse characteristics.

The solution of Laplace's equation is obtained using a boundary-integral method. The numerical procedure to solve the integral equations is presented in the next section. In these equations the incident stagnation-point flow ϕ_0 is defined to be

$$\phi_0(x, r) = \pm \frac{1}{2} c_0 (r^2 - 2x^2), \tag{5}$$

where the sign of c_0 determines whether we are considering a forward or rearward stagnation-point flow.

The initial conditions are taken from the spherically symmetric Rayleigh bubble solution in an infinite fluid for a bubble of small radius R_0 together with the corresponding axisymmetric stagnation-point flow on the surface of the bubble, as follows:

$$\phi(x, r, t_\epsilon) = \phi_0(x, r) + \phi_R(R_0, t_\epsilon), \tag{6a}$$

where
$$\phi_R(R_0, t_\epsilon) = -R_0 \left[\frac{2}{3} \left(\frac{\Delta P}{\rho} \right) \left\{ \left(\frac{R_m}{R_0} \right)^3 - 1 \right\} \right]^{\frac{1}{2}} \tag{6b}$$

and
$$t_\epsilon = 3R_m \left(\frac{3\rho}{2\Delta P} \right)^{\frac{1}{2}} B_a \left(\frac{5}{6}, \frac{3}{2} \right), \quad a = \left(\frac{R_0}{R_m} \right)^3. \tag{6c}$$

The 'initial time' t_ϵ is the time it takes a Rayleigh bubble to grow to radius R_0 from inception, which is expressed in terms of an incomplete beta function (Abramowitz

& Stegun 1965). The initial bubble potential ϕ_R may be modified slightly by the inclusion of the image source term but this only produces an $O((R_0/h)^2)$ change in ϕ and has no major significance during the stable growth phase.

Fluid particles remain on the surface of the bubble, thus yielding the kinematic condition

$$\frac{d\mathbf{x}}{dt} = \nabla\phi, \quad \mathbf{x} \in S, \quad (7)$$

i.e. the surface velocity of the bubble is equal to the fluid velocity. The dynamic condition on the bubble requires that the pressures be equated, which in the absence of surface-tension forces becomes

$$p_c = p_s - \rho \frac{\partial\phi}{\partial t} - \frac{1}{2}\rho |\mathbf{u}|^2 \pm \rho g x, \quad (8)$$

where p_c is the saturated vapour pressure inside the cavitation bubble, p_s is the undisturbed steady stagnation pressure and $|\mathbf{u}|$ is the magnitude of the velocity. The sign of the last term depends on the direction of the gravity vector. The remaining boundary condition that needs to be specified is the zero-normal-velocity condition on the rigid boundary,

$$\frac{\partial\phi}{\partial x} = 0 \quad \text{on } x = 0 \quad (9)$$

In developing the numerical solution of these equations it is convenient to scale all terms, thus producing dimensionless equations and, in doing so, yielding the dimensionless groups previously defined in (3). Thus all lengths are scaled with respect to the maximum bubble radius R_m yielding the following dimensionless quantities:

$$X = \frac{x}{R_m}, \quad R = \frac{r}{R_m}, \quad \gamma = \frac{h}{R_m}. \quad (10)$$

Quantities involving time either explicitly or implicitly are scaled with respect to

$$\hat{t} = \frac{R_m}{\left[\frac{p_0 - p_c}{\rho} \right]^{\frac{1}{2}}},$$

while the pressure and potentials are scaled as follows,

$$P = \frac{p - p_c}{p_0 - p_c}, \quad \Phi = \frac{\phi}{R_m} \left(\frac{\rho}{\Delta p} \right)^{\frac{1}{2}}, \quad \alpha = c_0 R_m \left(\frac{\rho}{\Delta p} \right)^{\frac{1}{2}}, \quad (11)$$

where α is clearly a measure of the strength of the axisymmetric stagnation-point flow and p_0 is the pressure at the initial location of the bubble prior to the generation of the bubble.

The dimensionless parameter δ arises from the dynamic boundary condition on the bubble surface which, after rearranging and reverting to lower-case notation, yields

$$\frac{\partial\phi}{\partial t} = 1 + \frac{1}{2}\alpha^2\gamma^2 - \frac{1}{2}|\mathbf{u}|^2 \pm \delta^2(X - \gamma). \quad (12)$$

Physically δ corresponds to the ratio of the half-life of the bubble to the time it takes a bubble of radius R_m to rise the order of one radius from rest due to buoyancy forces.

3. Numerical analysis

The boundary-integral method is used to solve the integral-equation formulation for the growth and collapse of a buoyant vapour bubble in the presence of an ambient axisymmetric stagnation-point flow and in the close proximity of a rigid boundary. The appropriate boundary-integral formulation that includes the incident stagnation-point flow is

$$c\phi = 4\pi\phi_0 + \int_S \left(\frac{\partial\phi}{\partial n} G - \phi \frac{\partial G}{\partial n} \right) dS, \tag{13}$$

where ϕ is the potential, $\partial\phi/\partial n$ the normal velocity with \mathbf{n} the outward normal, ϕ_0 the axisymmetric stagnation-point flow defined in (5) and

$$c(p) = \begin{cases} 4\pi & \text{if } p \in \Omega, \\ 2\pi & \text{if } p \in S, \end{cases} \tag{14}$$

where Ω is the domain of the fluid and S the bubble surface. In the case of a rigid boundary, the Green function consists of a source and an equal source at the image point, thus automatically satisfying the boundary condition specified in (9). As the problem is axisymmetric the Green functions may be integrated in the azimuthal direction leading to expressions involving complete elliptic integrals.

A Lagrangian description of the bubble surface S is employed. Thus the surface of the bubble (r, x) and the potential are specified at $N+1$ points requiring a representation for r, x, ϕ and $\partial\phi/\partial n$ on N segments. This is achieved by the following isoparametric approximation for both the surface and the functions. Thus on each segment S_j ($j = 1, \dots, N$) we have

$$\left. \begin{aligned} r(\xi) &= r_j M_1(\xi) + r_{j+1} M_2(\xi), \\ x(\xi) &= x_j M_1(\xi) + x_{j+1} M_2(\xi), \\ \phi(\xi) &= \phi_j M_1(\xi) + \phi_{j+1} M_2(\xi), \\ \psi(\xi) &= \psi_j M_1(\xi) + \psi_{j+1} M_2(\xi), \end{aligned} \right\} \tag{15a}$$

where the parameter ξ is in the range $(0, 1)$ and

$$\left. \begin{aligned} M_1(\xi) &= 1 - \xi, \\ M_2(\xi) &= \xi, \end{aligned} \right\} \tag{15b}$$

and also ψ is defined as $\partial\phi/\partial n$. It is assumed that ϕ_j and ψ_j are single-valued at the end points of the linear segments that approximate the surface.

Collocation points are chosen to be the end points of the N segments, yielding $N+1$ equations in $N+1$ unknowns of the form

$$2\pi\phi_i + \sum_{j=1}^N (a_{1ij}\phi_j + a_{2ij}\phi_{j+1}) = \sum_{j=1}^N (b_{1ij}\psi_j + b_{2ij}\psi_{j+1}), \tag{16}$$

where ϕ_i corresponds to the difference between the potential ϕ and the axisymmetric stagnation point potential ϕ_0 . The coefficients in (16) are obtained as follows;

$$a_{kij} = s_j \int_0^1 d\xi M_k(\xi) \int_0^{2\pi} \frac{\partial}{\partial n} \left\{ \frac{1}{|p_i - q(r, \theta)|} + \frac{1}{|p_i + \hat{q}(r, \theta)|} \right\} d\theta \tag{17}$$

and
$$b_{kij} = s_j \int_0^1 d\xi M_k(\xi) \int_0^{2\pi} \left\{ \frac{1}{|p_i - q(r, \theta)|} + \frac{1}{|p_i + \hat{q}(r, \theta)|} \right\} d\theta, \tag{18}$$

where s_j is the length of the segment and $\hat{q}(r, \theta)$ is the image point of $q(r, \theta)$ in the plane $x = 0$.

The integrals are performed analytically through the azimuthal angle $(0, 2\pi)$ to yield complete elliptic integrals and then numerically by using appropriate quadrature rules. Gauss–Legendre quadrature is adequate unless the collocation point p_i is within the segment s_j or is one of the end points, in which case the integrand is singular and must be treated specially. The singular integrals are performed by separating the integrals into the logarithmically singular term and the non-singular term. The singular term is integrated using a quadrature scheme incorporating the logarithm to complete the integration (Stroud & Secrest 1962) while the non-singular term uses normal Gauss–Legendre quadrature. The matrix equation (16) is solved using standard elimination packages to yield the normal velocity at the end of each segment.

The initial shape of the bubble will be taken to be a sphere of small radius R_0 (usually $R_0 \approx 0.1R_m$) located a distance h above the rigid boundary. We suppose the initial potential on the surface of the bubble due to its outward spherical motion is that associated with the equivalent Rayleigh bubble of the same radius. Account may be taken of the rigid boundary in the initial condition but it does not appear to be of great importance. With this initial information we may now solve (16) to yield the normal velocity $\partial\phi/\partial n$ on the bubble surface. With our prior knowledge of ϕ we may also calculate the tangential velocity on the bubble surface which, together with $\partial\phi/\partial n$, completely specifies the velocity ($\mathbf{u} = \nabla\phi$) of a ‘fluid particle’ on the surface of the bubble. This now enables us to ‘update’ the shape of the bubble and the potential on its surface at each of these points by using a simple Euler scheme as follows:

$$\left. \begin{aligned} r_j(t + \Delta t) &= r_j(t) + v_j \Delta t + O(\Delta t)^2, \\ x_j(t + \Delta t) &= x_j(t) + u_j \Delta t + O(\Delta t)^2, \\ \phi_j(r_j(t + \Delta t), x_j(t + \Delta t), t + \Delta t) &= \phi_j(r_j, x_j, t) + \left[\frac{\partial\phi}{\partial t} + |\mathbf{u}|^2 \right]_{(r_j, x_j, t)} \Delta t + O(\Delta t)^2. \end{aligned} \right\} \quad (19)$$

The $\partial\phi/\partial t$ in (19) may be replaced by using the Bernoulli pressure condition (8) on the bubble surface, thus allowing us to ‘update’ the potential on the bubble surface without requiring a finite-difference expression for $\partial\phi/\partial t$. The time step Δt is carefully chosen so as to restrict the change in ϕ . The above procedure is repeated throughout the growth and collapse of the bubble, yielding the time history of the bubble shape and the trajectories of all the particles. In addition, the pressure and velocity field may be calculated anywhere in the fluid during the lifetime of the bubble. More extensive details on the boundary-integral method used here may be obtained from Taib *et al.* (1984) and Taib (1985).

In the calculations, the results of which are described in the next section, N is equal to either 16 or 32. Accuracy tests were conducted on the spherically symmetric Rayleigh bubble problem on which an exact solution is available for comparison. Errors in the normal velocity ranged from 0.76% for the 16-point linear isoparametric representation through to 0.003% for the 16-point quadratic representation (Taib 1985). Computations were performed on the UNIVAC 1100/60 computer at the University of Wollongong Computer Centre.

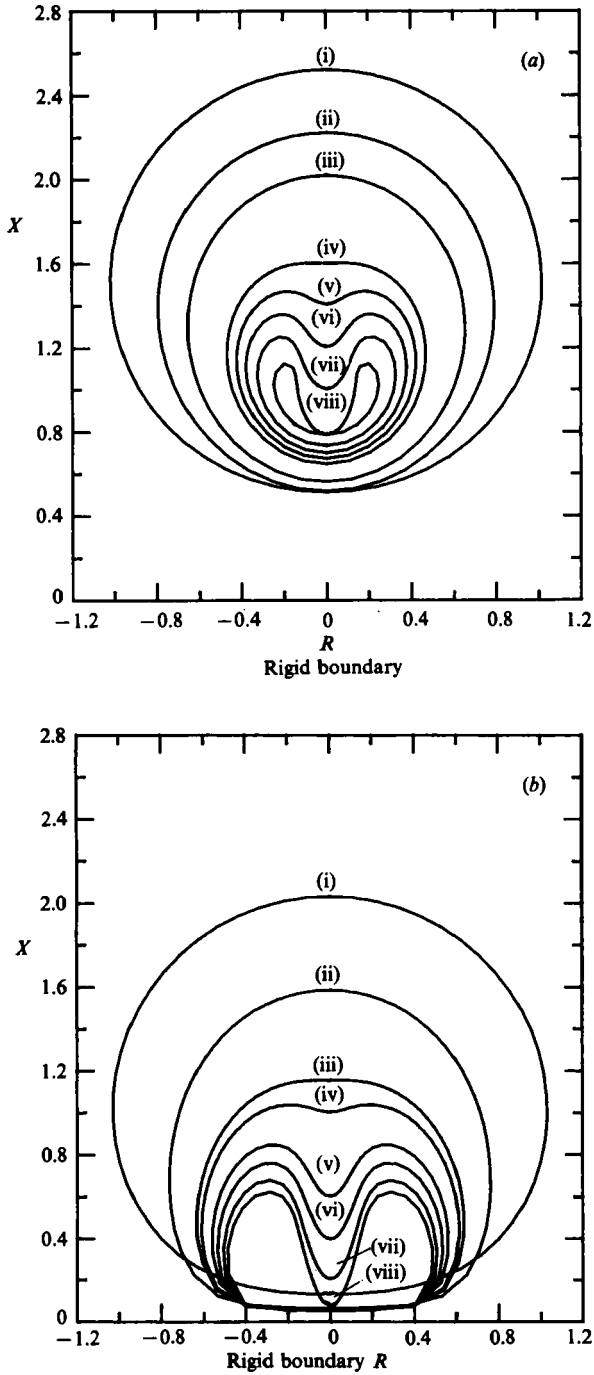


FIGURE 2. (a) Bubble shapes for $\gamma = 1.5$ during collapse phase at dimensionless times (i) 1.034, (ii) 1.725, (iii) 1.880, (iv) 2.015, (v) 2.039, (vi) 2.058, (vii) 2.077, (viii) 2.097. (b) Bubble shapes for $\gamma = 1.0$ during collapse phase at dimensionless times (i) 1.047, (ii) 1.856, (iii) 2.027, (iv) 2.053, (v) 2.102, (vi) 2.126, (vii) 2.449, (viii) 2.164.

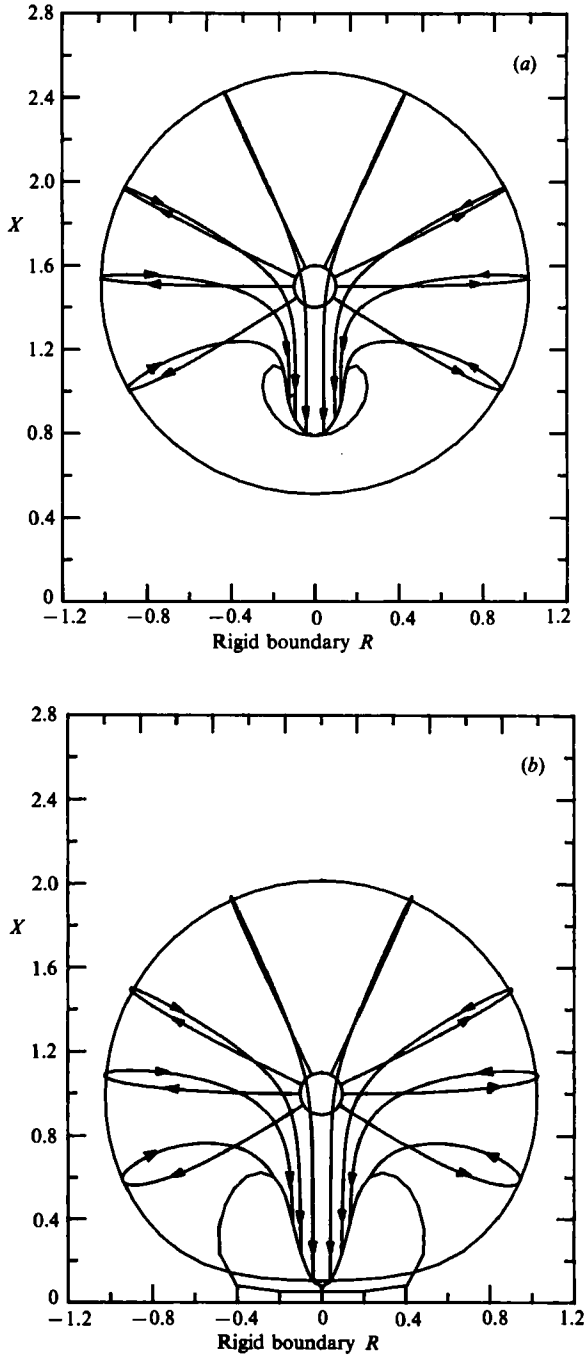


FIGURE 3. The particle pathlines during growth and collapse for the cases (a) $\gamma = 1.5$ and (b) $\gamma = 1.0$.

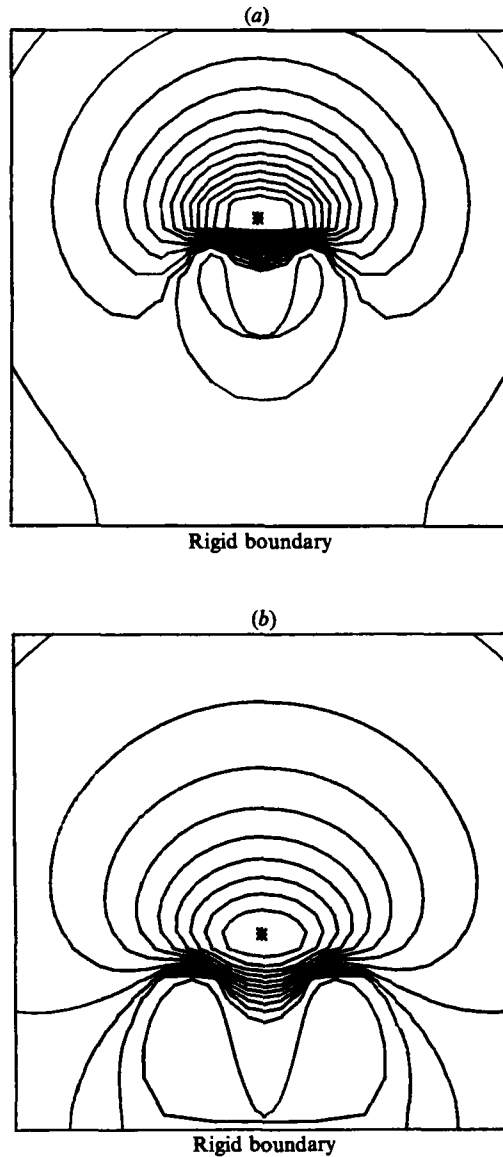


FIGURE 4. Equally spaced pressure contours for (a) $\gamma = 1.5$ at dimensionless time 2.097 and (b) $\gamma = 1.0$ at dimensionless time 2.164. Maximum pressure at (*) of 29.54 and 8.21 respectively.

4. Computational results

In this section we illustrate the bubble shape, particle paths and pressure contours that are predicted for the growth and collapse of a cavitation bubble near a rigid boundary. In the following discussion we will consider several separate examples that will assist us in gaining a firmer understanding of the growth and collapse of a cavitation bubble near a rigid boundary.

4.1. Rigid boundary

In figures 2, 3 and 4 examples of bubble shape, particle paths and final pressure contours are illustrated for $\gamma = 1.5$ and 1.0. In these examples gravity and an ambient incident flow are not included, leaving only the rigid boundary to break the spherical symmetry of the Rayleigh bubble. In figures 2(a, b) the bubble shape for the collapse phase is shown; in both cases yielding a high-speed jet directed towards the boundary. The closer the bubble is to the boundary, the more asymmetric is the collapse, the greater the volume of vapour left in the bubble as it becomes multiply connected and the greater the lifetime of the bubble. In addition if we compare our results with those of Plesset & Chapman (1971) and Prosperetti (1982), who only considered the collapse phase from a sphere, we find that our bubbles are significantly closer to the rigid boundary, indicating the importance of the growth phase in ultimately determining the collapse characteristics of the bubble.

Figure 3 illustrates the particle pathlines through both growth and collapse. During the growth phase, particle pathlines are almost radial, looping around near 'half-life' to be drawn down into the almost parallel motion found in the high-speed liquid jet.

Figure 4 shows the pressure contours at the last time step before the jet touches the free surface on the other side of the bubble. From the Rayleigh-bubble example we might anticipate a maximum pressure occurring close to the bubble surface and, because of the loss of spherical symmetry in the rigid boundary, we might expect either some axially symmetric surface, a ring or a point on the axis to be the 'region' of maximum pressure. In the case of a rigid boundary alone it proves to be a point on the axis above the bubble. A physical explanation is as follows: at the start of the collapse the maximum pressure occurs at infinity causing the fluid to accelerate towards the bubble, fluid preferentially being drawn from near the vertical axis because of the focusing effect of the rigid boundary. However as the collapse continues, mass conservation demands that the bulk of the fluid some distance from the boundary must decelerate, creating a point of maximum pressure (i.e. $\alpha \alpha \nabla p = 0$) close to the collapsing bubble surface. Conversely, the small volume of fluid between the point of maximum pressure and the bubble is being continually accelerated, creating the very high-speed liquid jet so clearly evident in figure 2.

It is of interest to calculate the maximum jet speed U_m which occurs at the end of the collapse phase. For $\gamma = 1.0$ the maximum speed of the jet is $U_m = 8.6(\Delta p/\rho)^{1/2}$, while $U_m = 11.0(\Delta p/\rho)^{1/2}$ for $\gamma = 1.5$, and at $\gamma = 2.0$ a value of $U_m = 16.1(\Delta p/\rho)^{1/2}$ is obtained. The higher jet speeds occur because the bubble has the opportunity to collapse to a smaller size, and hence higher velocities and pressures (see figure 4), for larger values of γ . Gibson (1968) calculated from his experiments an average value of $\bar{U}_m = 7.6(\Delta p/\rho)^{1/2}$ for values of γ around 1.0, thus confirming the general accuracy of our calculations.

4.2. Rigid boundary, buoyant bubble

While buoyancy is normally insignificant in transient cavitation bubbles, it may be important in experimental apparatus to study cavitation while operating under reduced pressure or in underwater explosions. However our main interest is due to the facility of gravity introducing a pressure gradient in the fluid but with the added advantage of the absence of fluid motion. It allows us a 'free parameter' in which we may vary the pressure gradient around the bubble to gain a better physical understanding of cavitation phenomena near a boundary.










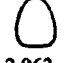









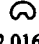














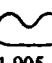
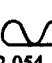



$\delta \backslash \gamma$	1.0			2.0		
0	 2.053	 2.126	 2.164	 2.010	 2.025	 2.035
0.158	—	—	—	 2.001	 2.028	 2.033
0.224	 2.063	 2.116	 2.120	 2.000	 2.028	 2.032
0.316	 2.051	 2.128	 2.178	 1.992	 2.016	 2.039
0.447	 1.647	 2.024	 2.117	—	—	—
-0.224	—	—	—	 1.959	 2.000	 2.034
-0.316	 1.899	 2.031	 2.127	 1.924	 1.999	 2.040
-0.447	 1.804	 1.905	 2.054	 1.823	 1.937	 2.044

FIGURE 5. Bubble shapes for buoyant vapour bubbles near a rigid boundary for indicated values of γ and δ .

In figure 5 the effects of buoyancy forces on the growth and collapse of a vapour bubble near a rigid boundary are illustrated for γ -values of 1 and 2 at varying values of δ . The positive sign for δ indicates that buoyancy forces acting on the bubble are directed away from the boundary whereas the negative sign indicates the reverse. Dimensionless times are indicated underneath the bubble shape.

The uppermost diagrams, corresponding to $\delta = 0$, show the various shapes in the absence of buoyancy forces (the $\gamma = 1$ example is identical to figure 2(b)), which are the shapes that will form the basis of comparison in the following discussion. For the positive δ -values buoyancy forces retard the motion of the bubble towards the boundary because they are acting in the opposite direction. In several examples ($\gamma = 2, \delta = 0.224, 0.316$) they dominate the motion, forcing the bubbles to migrate away from the boundary.

The $\gamma = 1$ examples yield a wide range of unusual bubble shapes. For this value of γ we would expect a strong Bjerknes attraction force towards the boundary, as is borne out by $\delta = 0$ example of figure 2(b) yielding a high-speed liquid jet in the

latter stages of collapse. The $\delta = 0.224$ example shows a much weaker jet structure than the $\delta = 0$ case because of the opposing buoyancy forces. The next two examples corresponding to $\delta = 0.316$ and 0.447 yield most unusual bubble shapes in the latter stages of collapse. The $\delta = 0.316$ calculations indicate a 'columnar'-shaped bubble that finally collapses towards the rigid boundary. In the $\delta = 0.447$ case buoyancy forces marginally dominate boundary attraction forces producing a 'light-bulb' shaped bubble, which is not uncommon in chemical bubble reactors (Pinczewski 1981). In the bottom two examples ($\delta = -0.316, -0.447$) buoyancy forces act towards the boundary in the same direction as the Bjerknes force. Two features are apparent in these examples. First, the bubbles are more oblate with a broader jet than the zero-buoyancy examples. Secondly, the lifetime of the bubble is less because the stronger buoyancy force pushes the jet through earlier, bearing out the intuitive ideas of Benjamin & Ellis (1966) who wrote that '... too large a normal motion may precipitate jet formation too early in the collapse for it to be most effective ...'.

In the $\gamma = 2$ example the Bjerknes force is much weaker and, as a consequence, produces much smaller, almost spherical bubbles yet with a small fast jet at the completion of the collapse phase (provided, of course, that the buoyancy forces are not too dominant, as occurs in the $\delta = 0.447$ example). The lifetime of the bubble appears to be relatively insensitive to either the magnitude or the sign of the buoyancy parameter. An interesting feature is the change in direction of migration of the bubble, and hence the direction of the liquid jet, in going from $\delta = 0.158$ to 0.224 . In the next section we provide a physical explanation of this phenomenon by introducing the concept of the Kelvin impulse. A significant-sized jet is produced towards the rigid boundary for the $\delta = -0.316$ and -0.447 examples when the buoyancy forces acting towards the boundary dominate the motion of the bubble.

4.3. *Rigid boundary, buoyant bubble, stagnation-point flow*

In figure 6 the additional influence of axisymmetric stagnation-point flow is included. The stagnation-point flow contributes to the deformation of the bubble via the two separate mechanisms, first through the velocity field and secondly through the pressure gradient, which decelerates the incident flow to yield a maximum pressure at the stagnation-point.

In the upper set of diagrams in figure 6 examples are shown of the calculated bubble shapes of a buoyant vapour bubble in relatively weak stagnation-point flow. For the $\gamma = 2$ examples, both forward ($\alpha > 0$) and rearward ($\alpha < 0$) stagnation-point flows with buoyancy forces acting away ($\delta > 0$) and towards ($\delta < 0$) the rigid boundary are exhibited. In the $\alpha = 0.15$ examples neither attraction or repulsion mechanisms dominate but instead the bubble collapses from the side pinching-off the bubble into two parts. This type of phenomenon has been previously reported in experimental studies by Gibson & Blake (1982) near flexible boundaries, and by Chahine (1983) when a cavitation bubble is located equally distant from two parallel plane boundaries. Several of these calculations are reminiscent of the bubble shape observations made by Ellis (1956) and reported later by Lauterborn & Hentschel (1985). It is postulated that the final collapsed state of the bubble may be two toroidal bubbles/ring vortices with opposite circulation.

The $\alpha = -0.15$ examples produce entirely different bubble shapes from the $\alpha = 0.15$ examples even though the dynamics in each case are identical (i.e. both the ambient buoyant and stagnation-point pressure fields). However, the kinematics of the bubble motion are different. In the $\alpha > 0$ examples the bubble is being decelerated in the direction of the rigid boundary whereas for $\alpha < 0$ the bubble is






















$\gamma = 2.0$						
$\delta \backslash \alpha$	0.15			-0.15		
0	 1.973	 2.009	 2.039	 1.943	 1.968	 1.995
0.224	 1.975	 2.006	 2.025	 1.895	 1.934	 1.987
-0.224	 1.969	 2.011	 2.041	 1.895	 1.930	 1.973
$\gamma = 5.0$						
$\delta \backslash \alpha$	0.5					
0	 0.967	 1.057	 1.144			

FIGURE 6. Bubble shapes for buoyant vapour bubbles in axisymmetric stagnation-point flow near a rigid boundary for indicated values of α , γ and δ .

being accelerated away from the boundary. Thus we can observe, for the larger bubbles in the $\delta = \pm 0.224$ examples, that the liquid jets are formed in the direction that the buoyancy forces are acting: away from the boundary in the $\delta = 0.224$ example, toward the boundary in the $\delta = -0.224$ case. In the latter stages of collapse the instability due to the acceleration of the interface leads to a liquid jet appearing at the rear of the bubble. Thus, in the $\delta = -0.224$ example, this instability acts in the same direction as the buoyancy-driven jet while in the $\delta = 0.224$ case an opposing jet is produced yielding the unusual phenomenon of jets at both ends of the bubble. Superimposed on all of these features is the weak Bjerknes attraction force which can be seen in the $\delta = 0$ case in the top-right-hand diagram.

In the lower diagram bubble shapes are shown for the case of stronger stagnation-point flow, with the bubble located at a much greater distance from the boundary. Because the bubbles are in a stronger flow field they flatten out forming an oblate shape as predicted by Miksis, Vanden-Broeck & Keller (1982) and Ryskin & Leal (1984) for rising bubbles. The weak yet broad, jet is directed away from the rigid boundary as the pressure gradient is acting in this direction.

5. Kelvin impulse

The Kelvin impulse is a particularly valuable dynamical quantity in unsteady fluid mechanics, being first used in the context of cavitation-bubble dynamics by Benjamin & Ellis (1966). It corresponds to the local momentum of the cavitation bubble and can therefore be used to determine aspects of the gross bubble motion. It is a function of time and may change sign giving the appearance of less restrictive properties than linear momentum of, say, a projectile. Other terminology has been used in other areas. For example McIntyre (1981) uses the term pseudo-momentum in his study of wave mechanics (see also Benjamin 1984 for further discussion).

The Kelvin impulse arises naturally from the study of the conservation of linear momentum. When considered in a half-space, the following relation for the Kelvin impulse I of a buoyant bubble is obtained:

$$I = \rho \int_S \phi \mathbf{n} \, ds = \int_0^t F(t) \, ds, \quad (20)$$

with

$$F(t) = \rho g V \mathbf{e}_x + \rho \int_{\Sigma_b} \left\{ \frac{1}{2} (\nabla \phi)^2 \mathbf{n} - \frac{\partial \phi}{\partial n} \nabla \phi \right\} ds, \quad (21)$$

where V is the volume of the bubble, S the bubble surface, Σ_b the surface of the rigid boundary and \mathbf{e}_x the unit vector in the x -direction. Thus the Kelvin impulse of the bubble depends on the buoyancy force and a 'force' exerted on the fluid by the rigid boundary.

If the bubble is taken a sufficient distance away from the boundary it may be represented approximately by a time-varying point source, especially as far as the integral in (21) is concerned. Thus, for source strength $m(t)$, we obtain (Blake & Cerone 1982) for the x -component of the 'force' F

$$F_x(t) = \rho g V - \frac{\rho m^2}{16\pi h^2}. \quad (22)$$

The surprising feature of this calculation is that the second term is independent of the sign of $m(t)$, i.e. the impulse is the same whether it is a source or sink. In addition we may exploit the Rayleigh bubble solution for $m(t)$, which for dimensionless quantities yields

$$m(t) = \pm 4\pi R^2 \left[\frac{2}{3} \left(\frac{1}{R^3} - 1 \right) \right]^{\frac{1}{2}}, \quad (23)$$

the sign depending on whether it is the growth or collapse phase of the bubble.

We may now evaluate $I_x(T_c)$, the final value of the x -component of the Kelvin impulse, where T_c is the total lifetime of a Rayleigh bubble ($T_c = 1.83 \dots$). This may be interpreted as the final bubble momentum and hence yields the direction of migration of the bubble. It may be shown that

$$I_x(T_c) = \frac{2\sqrt{6\pi R_m^5 (\rho \Delta p)^{\frac{1}{2}}}}{9h^2} [2\gamma^2 \delta^2 B(\frac{1}{6}, \frac{1}{2}) - B(\frac{7}{6}, \frac{3}{2})], \quad (24)$$

where $B(z, w)$ are beta functions (see Abramowitz & Stegun 1965). The zero-impulse curve may be obtained from equating $I_x(T_c)$ to zero, yielding

$$\gamma \delta = \left(\frac{B(\frac{7}{6}, \frac{3}{2})}{2B(\frac{1}{6}, \frac{1}{2})} \right)^{\frac{1}{2}} \approx 0.442. \quad (25)$$

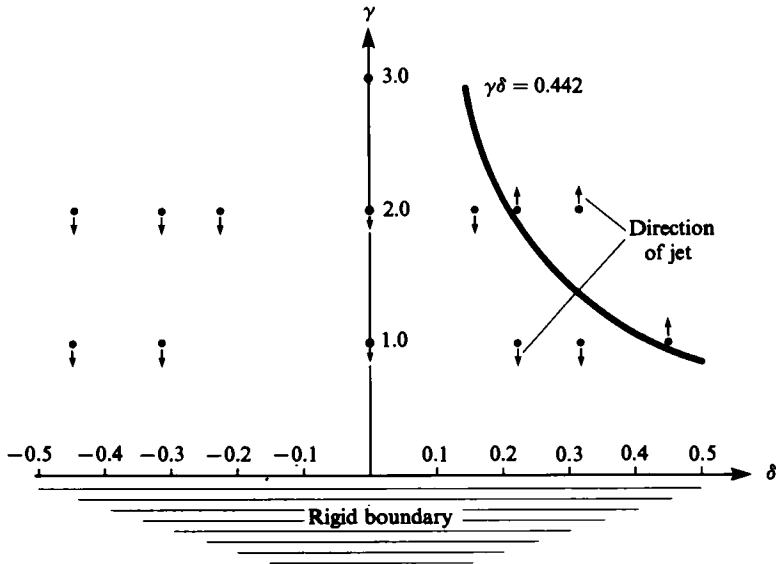


FIGURE 7. Graphical tabulation of numerical calculations conducted at different parameter values of γ and δ . The arrows indicate direction of jet and bubble migration. The null Kelvin-impulse line of $\gamma\delta = 0.442$ is included on the diagram.

Thus, if the parameters of the bubble are such that $\gamma\delta > 0.442$, the bubble will migrate away from the boundary as $I_x(T_c) > 0$, while if it is less than 0.442, the bubble will migrate towards the boundary. In our numerical experiments of the previous section, the results of which are summarized in figure 7, it would appear that (25) is an accurate estimate of the 'changeover condition' even when this approximation is not strictly valid close to the boundary (see e.g. figure 3).

In the absence of buoyancy forces or an ambient flow, a pulsating cavitation bubble is attracted towards a rigid boundary because of the Bjerknes effect. This is borne out by the Kelvin impulse which is directed towards the boundary during both growth and collapse of the bubble (αm^2 in (22)). In physical terms we may think in terms of the Kelvin impulse for the growth and collapse of a cavitation bubble as follows: during the growth phase the side of the bubble nearest the boundary will move into a region of higher relative impedance (i.e. larger added-mass) than the other side even though the velocities are similar. Thus the Kelvin impulse will be directed towards the boundary. Collapse occurs from the low-impedance side yielding the instability cum liquid jet on the far side of the bubble. A buoyancy force, proportional to bubble volume, when directed away from the boundary will slow the migration of the bubble and may even cause the bubble to migrate away from the boundary if sufficiently large. In this case the jet is often directed away from the boundary, as occurs in several of our examples.

6. Conclusion

In this paper we have considered the growth and collapse of a cavitation bubble near a rigid boundary in the presence of buoyancy forces and an incident stagnation-point flow. While a rigid boundary always attracts a pulsating cavitation bubble through the Bjerknes effect, buoyancy forces and stagnation-point flow may either attract or repel a bubble depending on their orientation and strength.

The sign and magnitude of Kelvin impulse appears to be a particularly valuable quantity in that it determines the direction of migration of the cavitation bubble and the violence with which it will collapse. It would appear that the Kelvin impulse of the collapsing cavitation bubble just prior to becoming multiply connected would need to be contained in the ring vortex system that is formed.

A pressure gradient directed away from the boundary slows the migration of the bubble towards the boundary and weakens the strength of the jet. Conversely, if the pressure gradient is directed towards the boundary, the collapsing bubble is more oblate and the jet slower and broader. The jet also forms earlier, shortening the lifetime of the bubble, and therefore may not be so damaging. It is clear that a set of optimal conditions exist for cavitation collapse to be most damaging and these remain to be determined.

Other features to come out of this study are (i) the importance of the growth phase in determining collapse characteristics; (ii) the initial location of the bubble; (iii) the relative strength of the buoyancy force and stagnation-point flow in determining collapse characteristics; (iv) the location of the regions of maximum pressure; and (v) the existence of a 'bubble-splitting' phenomena under certain conditions. It is clear that while a number of important features have been identified in this study, many more need to be studied to a greater depth especially with regard to fully three-dimensional flow.

The authors acknowledge the major contribution of Dr D. C. Gibson to our study of cavitation-bubble dynamics. The financial support given by the Government of Malaysia and the Universiti Pertanian Malaysia to Bachok bin Taib during his graduate studies at the University of Wollongong are gratefully acknowledged. Acknowledgement is also made of support from the Australian Research Grants Scheme.

REFERENCES

- ABRAMOWITZ, M. & STEGUN, I. A. 1965 *Handbook of Mathematical Functions*. Dover.
- ARNDT, R. E. A. 1981 Recent advances in cavitation research. *Adv. Hydrosci.* **12**, 1-78.
- BATCHELOR, G. K. 1967 *An Introduction to Fluid Dynamics*. Cambridge University Press.
- BENJAMIN, T. B. 1984 Impulse, flow force and variational principles. *IMA J. Appl. Maths.* **32**, 3-68.
- BENJAMIN, T. B. & ELLIS, A. T. 1966 The collapse of cavitation bubbles and the pressures thereby produced against solid boundaries. *Phil. Trans. R. Soc. Lond.* **A260**, 221-240.
- BIRKHOFF, G. & ZARANTONELLO, E. H. 1957 *Jets, Wakes and Cavities*. Academic Press.
- BLAKE, J. R. 1983 The Kelvin impulse: application to bubble dynamics. In *Proc. 8th Aust. Fluid Mech. Conf. Newcastle*. pp. 10B.1-10.B.4.
- BLAKE, J. R. & CERONE, P. 1982 A note on the impulse due to a vapour bubble near a boundary. *J. Aust. Math. Soc.* **B23**, 383-393.
- BLAKE, J. R. & GIBSON, D. C. 1981 Growth and collapse of a vapour cavity near a free surface. *J. Fluid Mech.* **111**, 123-140.
- CERONE, P. & BLAKE, J. R. 1984 A note on the instantaneous streamlines, pathlines and pressure contours for a cavitation bubble near a boundary. *J. Aust. Math. Soc.* **B26**, 31-44.
- CHAHINE, G. L. 1982 Experimental and asymptotic study of non-spherical bubble collapse. *Appl. Sci. Res.* **38**, 187-198.
- CHAHINE, G. L. & BOVIS, A. G. 1983 Pressure field generated by non spherical bubble collapse. *Trans. ASME* **105**, 356-363.
- ELLIS, A. T. 1956 Techniques for pressure pulse measurements and high speed photography in ultrasonic cavitation. In *Cavitation in Hydrodynamics*, Paper 8, pp. 1-32. HMSO, London.
- GIBSON, D. C. 1968 Cavitation adjacent to plane boundaries. In *Proc. 3rd Aust. Conf. on Hydraulic and Fluid Mechanics*, pp. 210-214. Institution of Engineers, Sydney, Australia.

- GIBSON, D. C. & BLAKE, J. R. 1982 The growth and collapse of bubbles near deformable surfaces. *Appl. Sci. Res.* **38**, 215–224.
- GUERRI, L., LUCCA, G. & PROSPERETTI, A. 1981 A numerical method for the dynamics of non-spherical cavitation bubbles. In *Proc. 2nd Int. Collog. on drops and bubbles, California*, pp. 175–181.
- HAMMITT, F. G. 1980 *Cavitation and Multiphase Flow Phenomena*. McGraw-Hill.
- KNAPP, R. T., DAILY, J. W. & HAMMITT, F. G. 1970 *Cavitation*, McGraw-Hill.
- LAMB, H. 1932 *Hydrodynamics*. Cambridge University Press.
- LANDWEBER, L. & MILOH, T. 1980. Unsteady Lagally theorem for multipoles and deformable bodies. *J. Fluid Mech.* **96**, 33–46.
- LAUTERBORN, W. 1982 Cavitation bubble dynamics – new tools for an intricate problem. *Appl. Sci. Res.* **38**, 165–178.
- LAUTERBORN, W. & BOLLE, H. 1975 Experimental investigations of cavitation bubble collapse in the neighbourhood of a solid boundary. *J. Fluid Mech.* **72**, 391–399.
- LAUTERBORN, W. & HENTSCHEL, W. 1985 Cavitation bubble dynamics studied by high speed photography and holography. Part I. Ultrasonics (in press).
- LAUTERBORN, W. & VOGEL, A. 1984 Modern optical techniques in fluid mechanics. *Ann. Rev. Fluid Mech.* **16**, 223–244.
- LENOIR, M. 1976 Calculations numerique le l'implosion d'une bulle de cavitation au voisinage d'une paroi ou d'une surface libre. *J. Mech.* **15**, 725–751.
- MCINTYRE, M. E. 1981 On the 'wave momentum' myth. *J. Fluid Mech.* **106**, 331–347.
- MIKSIS, M. J., VANDEN-BROECK, J. M. & KELLER, J. B. 1982 Rising bubbles. *J. Fluid Mech.* **123**, 31–42.
- PINCZEWSKI, W. W. 1981 The formation and growth of bubbles at a submerged orifice. *Chem. Engng. Sci.* **36**, 405–411.
- PLESSET, M. S. & CHAPMAN, R. B. 1971 Collapse of an initially spherical vapour cavity in the neighbourhood of a solid boundary. *J. Fluid Mech.* **47**, 283–290.
- PROSPERETTI, A. 1982 Bubble dynamics: a review and some recent results. *Appl. Sci. Res.* **38**, 145–164.
- RAYLEIGH, LORD 1917 On the pressure developed in a liquid during the collapse of a spherical void. *Phil. Mag.* **34**, 94–98.
- RYSKIN, G. & LEAL, L. G. 1984 Numerical solution of free-boundary problems in fluid mechanics. Part 2. Buoyancy-driven motion of a gas bubble through a quiescent fluid. *J. Fluid Mech.* **143**, 19–36.
- SAFFMAN, P. G. 1967 The self propulsion of a deformable body in a perfect fluid. *J. Fluid Mech.* **28**, 385–389.
- STROUD, A. H. & SECREST, D. 1966 *Gaussian Quadrature Formulas*. Prentice Hall.
- TAIB, B. B. 1985 Boundary integrals methods applied to cavitation bubble dynamics. PhD thesis, University of Wollongong.
- TAIB, B. B., DOHERTY, G. & BLAKE, J. R. 1984 Boundary integral methods applied to cavitation bubble dynamics. In *Mathematical Programming and Numerical Analysis Workshop* (eds S. A. Gustafson & R. S. Womersley,), vol. 6, pp. 166–186. Centre for Math. Anal. A.N.U.
- WU, T. Y. 1976 The momentum theorem for a deformable body in a perfect fluid. *Schiffstechnik* **23**, 229–232.